WEP Warwick Evans Publishing

International Journal of Materials Science and Technology Studies

ISSN: 3006-7693 (Print), ISSN: 3006-3744 (Online) | Volume 4, Number 1, Year 2025
DOI: https://doi.org/10.62051/ijmsts.v4n1.03
Journal homepage: https://wepub.org/index.php/IJMSTS/index

Study on Microstructure Formation and Numerical Simulation of Cu-Sn Alloy in Ultrasonic-Assisted Laser Soldering Process

Xinlei Wei *, Guoqing Cai, Shaoyang Zhu, Guoqing Mei

School of Intelligent Manufacturing, Wenzhou Polytechnic, Wenzhou 325000, China
*Corresponding Author: Xinlei Wei

ABSTRACT

To reveal the microstructure formation mechanism of Cu-Sn alloy and the synergistic effect law of composite energy fields in the ultrasonic-assisted laser soldering process, this study employed a combination of experimental and numerical simulation methods to systematically investigate the effects of laser power (5-20W) and ultrasonic frequency (0-40kHz) on the temperature field, flow field, growth of interfacial intermetallic compounds (IMC), and reliability of solder joints. The experiment utilized a semiconductor laser system and an ultrasonic auxiliary device, and combined with COMSOL multiphysics simulation to construct a laser-ultrasonic composite energy field model, focusing on analyzing molten pool convection, temperature distribution, creep strain, and failure cycle characteristics. The results show that laser power dominates heat input and determines the energy accumulation state of the molten pool; ultrasonic frequency regulates molten pool flow through acoustic streaming effect, with around 30kHz achieving optimal momentum transfer, significantly improving temperature uniformity and refining the IMC layer; the synergy of high power (15-20W) and ultrasound (30-40kHz) can enhance the wettability and spreadability of solder joints, but excessively high ultrasonic frequency (40kHz) easily causes solder splashing. Accelerated life test simulations indicate that the interfacial region experiences creep strain concentration due to thermal mismatch, which is the weak link of fatigue failure, and ultrasonic assistance can extend the service life of solder joints by reducing the energy dissipation rate. This study clarifies the matching mechanism of laser-ultrasonic parameters, providing a theoretical basis for optimizing high-reliability soldering processes in electronic packaging.

KEYWORDS

Ultrasonic-assisted laser soldering; Cu-Sn alloy; Molten pool flow; Solder joint reliability

1. INTRODUCTION

A Electronic manufacturing and assembly technology accurately assembles various packaged electronic components to designated positions on integrated circuit boards according to circuit design requirements, and ensures that solder joints meet welding quality standards, thereby satisfying the functional requirements of integrated circuits [1-2]. Under the stringent requirements of green environmental protection and lead-free soldering standards, traditional connection technologies for electronic devices on integrated circuit boards are constrained by technical bottlenecks such as limited contact methods, large heat-affected zones, and insufficient process controllability, making it difficult to meet the service performance indicators required for integrated circuit board packaging, such as fatigue resistance, tensile and shear resistance, and high toughness [3-4].

With the iterative development of industrial technology, laser soldering technology has gradually become a research hotspot due to its prominent advantages: welding accuracy can reach the micron

level, processing time can be programmatically controlled, the local heating method greatly reduces the heat-affected zone, and it can effectively eliminate electrostatic threats, thus showing unique applicability in the field of electronic product soldering [5]. Nishikawa et al. further confirmed that the impact reliability of solder joints prepared by the laser reflow process is better than that of the traditional reflow process, and the intermetallic compound (IMC) formed at the SAC/Cu interface is thinner [6], providing strong support for the performance advantages of laser soldering.

In terms of process mechanism research, Kunwar et al. combined laser soldering experiments, finite element analysis, and machine learning to build a data-driven model to predict the interfacial IMC morphology of the Sn-xAg-yCu/Cu (SAC/Cu) system. By processing SAC solder with different Ag and Cu ratios using a fiber laser at different powers and scanning speeds, two typical IMC morphologies, prismatic and fan-shaped, were found [7]. Bachok et al. focused on the reliability of laser soldering in the connection between pin-through-hole (PTH) components and printed circuit boards (PCB), and used Ansys Fluent software with the finite volume method (FVM) to simulate the solder flow process, revealing the influence of SAC305 solder volume on the fillet shape, pressure, and velocity of the through-hole capacitor and PCB connection [8].

However, the Gaussian distribution of the laser heat source easily leads to uneven heat distribution in the weld pool, affecting the quality of solder joints. To this end, Kago et al. proposed an ultrasonic-assisted reflow soldering process, which melts the solder by applying ultrasonic vibration to the printed circuit board (PCB). It not only does not require an additional heating source but also can improve the hardness and shear strength of solder joints by refining the solder matrix structure and thinning the interfacial IMC [9]. Yang et al. found that ultrasonic vibration can change the surface energy and capillary wave intensity of molten solder, promote the extension of the precursor film, and achieve effective wetting even in non-wetting systems [10]. However, existing studies mostly focus on the feasibility of ultrasonic-assisted welding and the impact on joint performance, with insufficient discussion on the interfacial reaction mechanism, especially the lack of a systematic understanding of the synergistic mechanism between ultrasound and laser soldering.

In view of this, this paper aims to reveal the mechanism of ultrasound in laser soldering through ultrasonic-assisted laser soldering experiments and numerical simulations, focusing on investigating the influence of different ultrasonic frequencies on temperature transfer, sound pressure distribution, interfacial IMC growth, and thermal failure behavior during the soldering process.

2. EXPERIMENTS AND NUMERICAL SIMULATION

2.1. Experimental Design

As shown in Figure 1, the laser welding system consists of a semiconductor laser (λ=915nm), an infrared thermometer, a LIBS system, an ultrasonic auxiliary device, and an automatic wire feeding device. The maximum output power of the laser is 50W, the focal length is 100mm, and the focused spot diameter is 0.65mm. The solder used is SnCu0.7 welding wire with a diameter of 1.2mm and a flux content of 2.2% (wt%). A double-sided copper-clad FR-4 printed circuit board was used as the substrate. The laser welding process is as follows: at 0s, the wire feeding device starts to feed the welding wire, and the laser system emits laser light at the same time. The welding wire is heated and melted to spread. At 1.0s, the wire feeding process ends, and the welding wire starts to retract. The molten solder continues to be heated and spread under the continuous laser irradiation (1.0-1.3s). During this process, the ultrasonic vibration parameters are controlled and output by an adjustable frequency ultrasonic generator, and transmitted to the molten solder through air at a given distance via an ultrasonic transducer with a diameter of 16mm. An infrared thermometer is used to measure and count the temperature of the solder joint in real-time. The parameters of ultrasonic-assisted laser soldering are shown in Table 1.

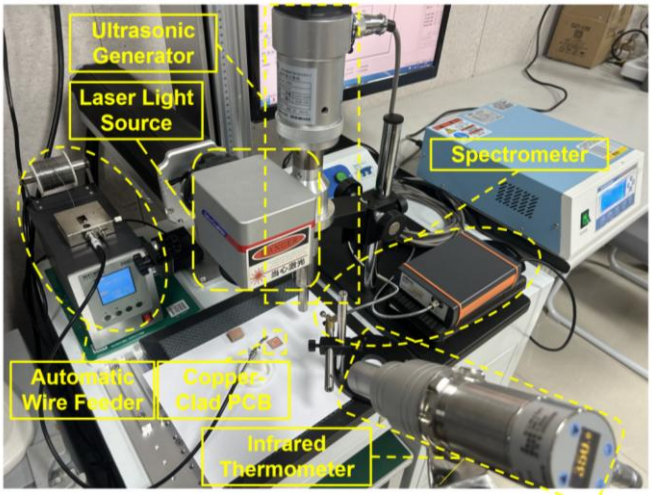

Figure 1. Ultrasonic-assisted laser soldering system

Table 1. Parameters of ultrasonic-assisted laser soldering

Parameter Name	Parameter Value
Laser power	5~20W
Spot diameter	1mm
Defocus amount	15mm
Ultrasonic frequency	0, 20~40kHZ
Soldering time	2s

2.2. Numerical Simulation

The finite element software COMSOL was used to simulate the ultrasonic-assisted laser soldering process, whose core is the coupling of laser heat source and ultrasonic vibration energy, which needs to consider both the heat input of the laser and the dynamic stress/additional thermal effect caused by ultrasound. Its core mechanisms are: (1) Enhancement of molten pool convection: ultrasonic acoustic streaming breaks the thermal boundary layer of the molten pool, making the temperature distribution more uniform (suppressing microcracks caused by local overheating); (2) Promotion of interfacial spreading: ultrasonic vibration reduces the surface tension of the solder, increases the cosine value of the contact angle, and improves the spreadability of the molten solder on the pins/solder joints (reducing cold solder joints and bridging); (3) Refinement of microstructure: acoustic streaming disturbance inhibits grain coarsening and promotes the uniform growth of the IMC layer, improving the joint strength.

2.2.1. Laser Heat Source Model

A surface heat source model is generally used as the laser heat source, and its energy density distribution can be defined as a Gaussian heat source. The corresponding heat flux density distribution is as follows:

$$Q_{laser}(x,y,t)=\frac{3Q_1}{\pi R_1^2}\exp\left(-\frac{3\left[(x-x_0)^2+(y-y_0)^2\right]}{R_1^2}\right)\cdot H(t) \quad (1)$$

Where, Q_{laser} is the laser power density at any point (x, y) in space at time t; Q_1 is the total laser power (W); R_1 is the spot radius (defined as the point where the intensity drops to 5% of the peak value); (x_0,y_0) is the coordinates of the spot center; (x,y) is the coordinate of any point in space, used to calculate the laser energy distribution at that point; H(t) is the time step function (1 for continuous laser, pulse waveform for pulsed laser).

2.2.2. Hydrodynamic Model of Ultrasonic Acoustic Streaming Effect

Ultrasonic vibration assists the flow of molten solder through acoustic streaming effect and cavitation effect, mainly affecting molten pool dynamics (wettability, convective mixing, interfacial reaction). Ultrasonic vibration drives molten pool flow through acoustic pressure gradient, satisfying the Navier-Stokes equation, and the power source is provided by the ultrasonic stress field:

$$\rho\left(\frac{\partial u}{\partial t}+u\cdot\nabla u\right)=-\nabla p+\mu\nabla^2 u+F_{ultra} \tag{2}$$

$$F_{ultra}=\rho_2\frac{\partial u_{lutra}}{\partial t} \tag{3}$$

$$u_{ultra}=A\cdot 2\pi f\cos(2\pi ft)\cdot n \tag{4}$$

Where, p is the fluid pressure, describing the pressure distribution in the molten pool; u is the dynamic viscosity of liquid tin, characterizing the fluid's resistance to shear deformation (the larger the value, the worse the fluidity); F_{ultra} is the ultrasonic volume force, the driving force generated by ultrasonic vibration on the molten pool; u_{ultra} is the ultrasonic vibration velocity vector.

2.2.3. Heat Transfer Model of Composite Energy Field

Considering the forced convection caused by ultrasonic acoustic streaming in the molten pool, its transient heat conduction equation is:

$$\rho c_p\frac{\partial T}{\partial t}=\nabla\cdot(\lambda\nabla T)+Q_{laser}+\rho c_p u\cdot\nabla T+L\rho\frac{\partial f_s}{\partial t} \tag{5}$$

Where, $\rho c_p u\cdot\nabla T$ is the convective heat transfer term caused by ultrasonic acoustic streaming, and u is the molten pool flow velocity (driven by ultrasonic vibration). L is the latent heat of fusion of the solder, and f_s is the solid fraction (describing the solid-liquid transformation).

2.2.4. Interfacial Reaction Model

Ultrasound promotes the interfacial reaction between the solder and the substrate. The growth kinetics equation of intermetallic compounds (IMC) is:

$$\frac{d\delta}{dt}=K_0\exp\left(-\frac{Q_{act}}{RT}\right)\cdot(1+\alpha\cdot Af) \tag{6}$$

Where, δ is the thickness of the IMC layer; K_0 is the frequency factor, related to the intrinsic rate of the interfacial reaction; Q_{act} is the activation energy, the energy barrier required for interfacial atomic diffusion or chemical reaction (the smaller the value, the easier the reaction); R is the gas constant, a fundamental thermodynamic constant; T is the absolute temperature, affecting the atomic diffusion rate (the higher the temperature, the faster the reaction); α is the ultrasonic enhancement coefficient, characterizing the promoting effect of ultrasonic amplitude A and frequency f on the interfacial reaction (positively correlated).

2.2.5. Boundary Conditions

(a) Thermal boundary: For the laser-irradiated surface, $-\lambda\frac{\partial T}{\partial n}=Q_{laser}$; For non-irradiated surfaces, convective heat dissipation occurs, $\lambda\frac{\partial T}{\partial n}=\alpha(T-T_{env})$,

(b) Fluid boundary: For the ultrasonic vibration surface, $u=u_{ultra}$, (vibration velocity directly drives the molten pool); For the solid-liquid interface: no-slip condition $u=0$ (the flow velocity in the solid phase region is 0).

(c) Wettability boundary: $\cos\theta=\frac{\gamma_{sv}-\gamma_{sl}}{\gamma_{1v}}\cdot(1+\beta\cdot Af)$, where θ is the contact angle, measuring the spreadability of the molten solder on the substrate; γ_{sv} is the solid-vapor interfacial tension, the surface energy between the substrate and gas; γ_{sl} is the solid-liquid interfacial tension, the surface energy between the substrate and molten solder; γ_{1v} is the liquid-vapor interfacial tension, the surface energy between the molten solder and gas; β is the ultrasonic wettability enhancement factor, positively correlated with materials and ultrasonic parameters.

3. RESULTS AND DISCUSSION

3.1. Loading Model

As shown in Figure 2, the ultrasonic-assisted laser soldering model consists of a SnCu solder layer on the top, a copper-clad layer in the middle, and an FR-4 layer at the bottom. The laser heat source acts directly above the middle part of the SnCu solder layer, and the ultrasonic vibration loading is set at the bottom of the FR-4 layer. The solid-liquid interface (the contact area between the SnCu solder layer and the copper-clad layer) is locally refined, and then the thermo-fluid-solid coupling simulation analysis under ultrasonic excitation is carried out.

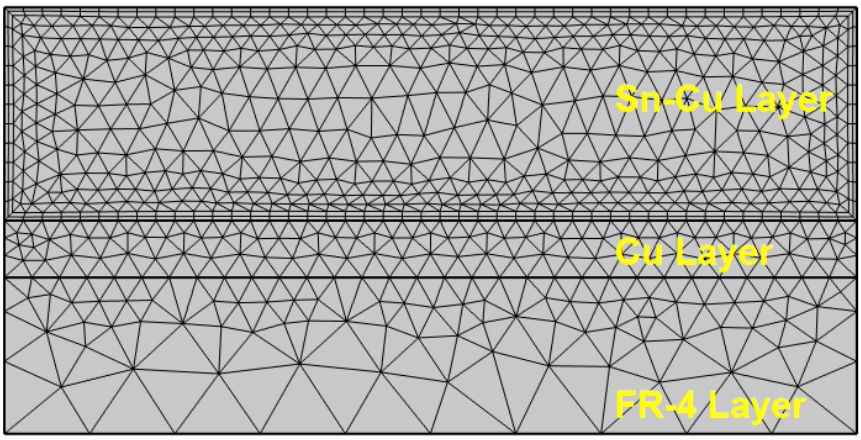

Figure 2. Ultrasonic-assisted laser soldering model

3.2. Multi-parameter Coupling Analysis of Temperature and Flow Velocity Characteristics in Ultrasonic-assisted Laser Soldering

Taking the laser power (5W, 10W, 15W, 20W) as the energy input variable and the ultrasonic frequency (0kHz, 20kHz, 30kHz, 40kHz) as the dynamic control variable, this study investigated the variation laws of the temperature distribution and flow velocity characteristics of the molten pool during the ultrasonic-assisted laser soldering process by comparing the temperature field and flow field characteristics under different parameter combinations, aiming to reveal the synergistic mechanism of the composite energy field.

Ultrasonic frequency / Laser power	f=0kHz	f=20kHz	f=30kHz	f=40kHz
P=5W	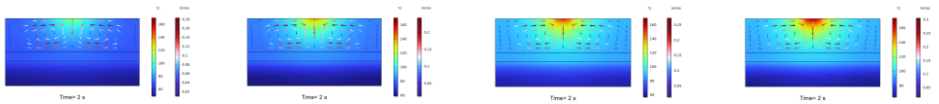			
P=10W	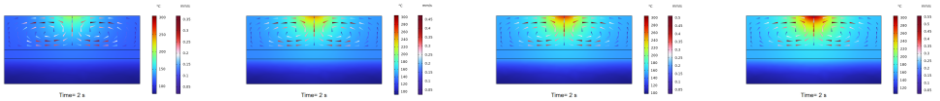			
P=15W	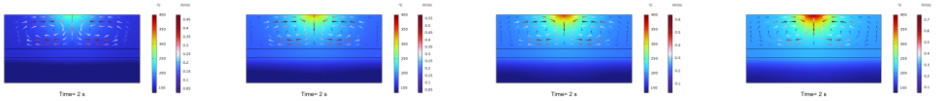			
P=20W	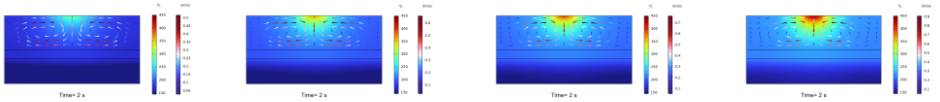			

Figure 3. Flow velocity distribution of thermal flow field under different ultrasonic frequencies and laser powers

3.2.1. Dominant Role of Laser Power in Temperature and Flow Velocity

Under the same ultrasonic frequency, as the laser power increases from 5W to 20W, the maximum temperature of the molten pool shows a significant upward trend. Without ultrasonic (0kHz) action, when the laser power is 5W, the corresponding maximum temperature is approximately 111.47°C, while under 20W laser, the maximum temperature rises to 291.79°C, confirming that laser power is the core driving factor for heat input and directly determines the energy accumulation level of the molten pool. The natural convection of the molten pool is enhanced under high power (due to buoyancy driven by the increased temperature gradient), but the increase in flow velocity is limited without ultrasound, indicating that pure heat-driven convection has a weak stirring effect on the molten pool, which easily leads to uneven temperature distribution (local overheating may occur). Without ultrasound (0kHz), when the laser output power is 5W, the peak flow velocity is approximately 0.18mm/s (weak natural convection); when the laser output power is 20W, the peak flow velocity is approximately 0.52mm/s (natural convection is enhanced due to the increased temperature gradient, but still weak). Natural convection under high power is prone to "local heat accumulation", and since heat cannot diffuse quickly, it may cause overheating oxidation of the solder or thermal damage to the substrate.

3.2.2. Dynamic Regulation Effect of Ultrasonic Frequency

Under the same laser power, after introducing ultrasonic vibration, the flow velocity of the molten pool increases significantly, and shows a trend of first increasing and then stabilizing with the increase of frequency. When the laser output power is 10W and the ultrasonic frequency is 0kHz, the peak flow velocity of the solder is approximately 0.37mm/s; at 20kHz, it increases to 0.47mm/s; at 30kHz, it reaches 0.51mm/s; at 40kHz, it remains at a similar level. This phenomenon is consistent with the mechanism of ultrasonic acoustic streaming effect, that is, ultrasonic vibration drives the flow of molten pool fluid through periodic pressure fluctuations, and around 30kHz may be close to the resonance frequency of the molten pool, at which time the momentum transfer efficiency is the highest.

Ultrasonic convection significantly improves the temperature distribution. For example, when the laser output power is 20W and the ultrasonic frequency is 0kHz, the temperature is concentrated in the range of 200-300°C (local high-temperature areas are obvious), while under the action of 30kHz ultrasound, the temperature range expands to 130-400°C, and the range of high-temperature areas shrinks. The reason may be that ultrasonic forced convection breaks the thermal boundary layer

formed by natural convection, making the heat diffuse more uniformly from the laser action center to the surrounding area. The mechanical stirring effect of ultrasound promotes heat diffusion, reduces the thermal gradient, and suppresses local overheating (reducing the risk of defects such as microcracks and pores).

Threshold effect: At low laser power (5W), the influence of ultrasound on temperature is weak because the overall temperature of the molten pool is low, and the heat dissipation effect of ultrasonic convection is not obvious; at high power (15W, 20W), the cooling and homogenization effects of ultrasound are more significant, indicating that ultrasonic assistance is more practical in high-energy input scenarios. When the ultrasonic frequency is 30kHz, the flow velocity and convective heat transfer efficiency reach the peak, and there is no significant improvement at 40kHz (for example, when the laser power is 20W, the flow velocity at ultrasonic frequencies of 30kHz and 40kHz is both about 0.9mm/s). This is because the efficiency of converting ultrasonic energy into fluid kinetic energy has a critical value, and excessively high frequency is prone to energy dissipation.

3.2.3. Synergistic Optimization Relationship Between Laser Power and Ultrasonic Frequency

Low power (5W): The laser heat input is limited, and ultrasonic forced convection becomes dominant. At 20-30kHz, the flow velocity increases from 0.24mm/s to 0.27mm/s, and convective heat transfer expands the temperature distribution from a "narrow range" to a "wide range", avoiding local cold soldering.

Medium power (10W, 15W): The heat input and forced convection are balanced, and convective heat transfer is optimal at 30kHz. For example, when the laser output power is 10W and the ultrasonic frequency is 30kHz, the flow velocity reaches 0.74mm/s, and the temperature distribution is uniform, which not only ensures the melting of the solder (>232°C) but also avoids local overheating.

High power (20W): It is necessary to balance heat input and ultrasonic heat dissipation. 40kHz ultrasound can maintain a flow velocity of 0.7-0.8mm/s, and the convective heat transfer coefficient is the highest, reducing the proportion of high-temperature areas (>400°C) from 30% at 0kHz to 10%, thereby suppressing solder burnout.

3.3. Accelerated Life Test of Solder Joints

3.3.1. Analysis of Solder Joint Creep Strain

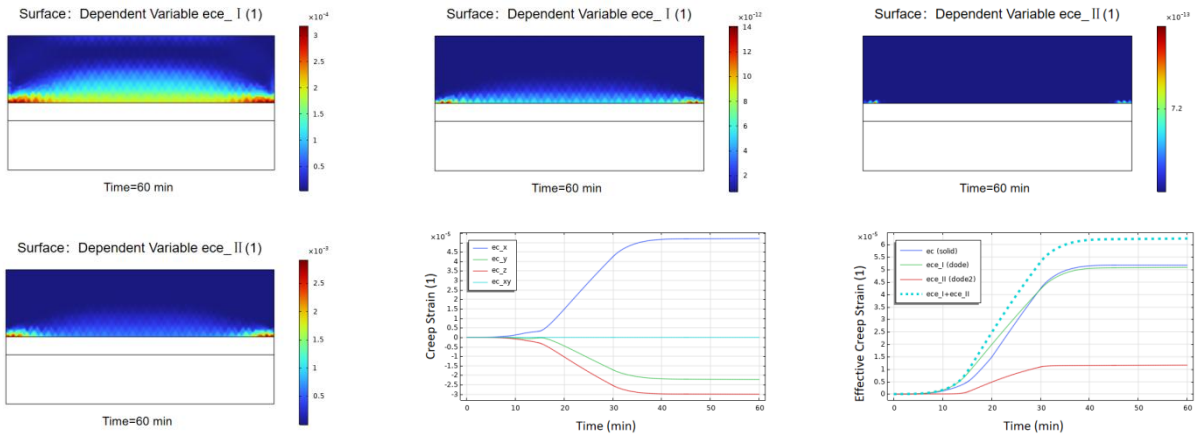

Figure 4. Multi-scale analysis of solder joint creep strain

To predict the fatigue life of solder joints under thermal load cycles, a fatigue simulation of accelerated life test solder joints was performed on the model. In the surface diagrams shown in Figure 4, creep strain is concentrated at the bottom interface of the solder joint (the colored area below in the figure), which conforms to the mechanical law of "geometric constraint + thermal mismatch":

during thermal cycling, the substrate is fixed, the bottom of the solder joint is constrained, the top is free, and the shear/tensile stress at the interface is amplified; the high hardness of the IMC layer at the interface leads to stress concentration, further promoting creep. In the edge regions of the interface (left and right sides) in Figures 4-1 and 4-4, the strain is higher than that in the center, confirming the edge stress concentration due to geometric constraints: the bottom of the solder joint is constrained by the substrate, and the shear stress at the edge is amplified, accelerating grain boundary sliding and creep damage.

In addition, from the dimensions of spatial distribution and temporal evolution, the prediction mechanism of solder joint creep damage is further constructed: the surface diagrams in Figures 4-1, 4-2, 4-3, and 4-4 show that the intragranular and intergranular creep strains in the solder joint-substrate interface and edge regions are much higher than those in the solder matrix (with an order of magnitude difference of 10^3-10^9), clarifying that the interface is the core area where fatigue cracks initiate; the time curves in Figures 4-5 and 4-6 reveal that creep undergoes a transition from "transient hardening to steady-state equilibrium" (with 20 min as the critical node), and intragranular/intergranular creep act synergistically, reflecting the anisotropic strain accumulation law under thermal mismatch stress. Combined with the double Norton model, these data can quantitatively analyze the damage rates in different regions (interface/matrix) and different stages (transient/steady-state), providing support for the design of temperature cycle parameters (frequency, temperature amplitude) in accelerated life tests and the calibration of multiple fatigue criteria (such as Coffin-Manson). Finally, it is clarified that the high-strain region of the interface is the life bottleneck, guiding the improvement of strain distribution through means such as optimizing the IMC layer and ultrasonic assistance to enhance the reliability of solder joints.

3.3.2. Analysis of Solder Joint Failure Cycle Number

Figure 5 shows the failure cycle number diagram (energy method, strain-life method), revealing that the solder joint-substrate interface and edge regions are the life bottlenecks (red low-cycle regions), which are strongly correlated with the previously high-concentration regions of creep strain, verifying the mechanical logic of "strain/energy concentration → damage accumulation → life attenuation". Because the energy method incorporates laser heat dissipation, the predicted interface life is shorter (lower limit of 10^4 cycles), reflecting the acceleration effect of thermal-mechanical composite loads; the strain-life method focuses on mechanical strain, with a higher upper limit of life (up to 10^{10} cycles), which is suitable for pure temperature cycle scenarios. They are complementary, clarifying that the interface edge is the core region for crack initiation, guiding the accelerated test to focus on observing this region, and distinguishing the damage contributions of thermal energy consumption and mechanical strain through model cross-validation, supporting the optimization of solder joint design (such as interface modification, geometric constraint regulation) and improving the accuracy and reliability of life prediction.

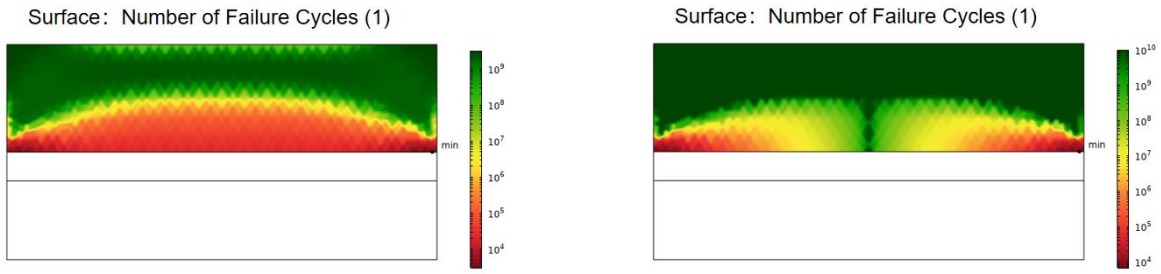

Figure 5. Analysis of solder joint failure cycle number

3.3.3. Analysis of Solder Joint Dissipation Energy

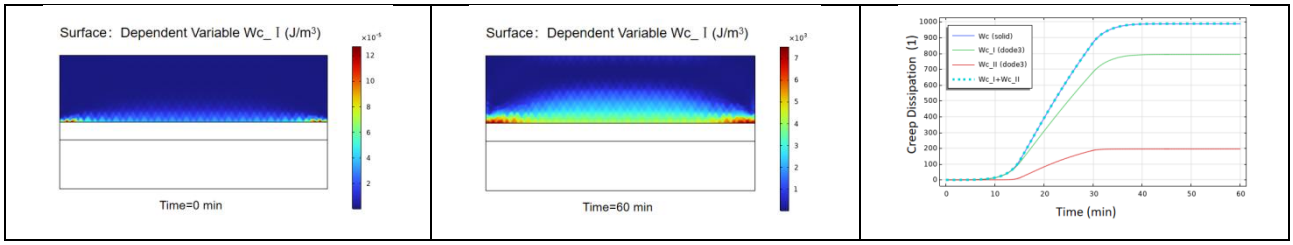

Figure 6. Distribution and historical change curve of creep dissipation energy of solder joints at different times

For the distribution and temporal evolution curve of creep dissipation energy at different times, the energy-driven mechanism of solder joint life degradation is revealed from the perspectives of spatial distribution and temporal evolution of creep dissipation energy: In Figure 6-1 (0 min), the dissipation energy at the solder joint-substrate interface is extremely low (on the order of 10^{-5}), while in Figure 6-2 (60 min), the interface dissipation energy surges to the order of 10^{3}, clearly indicating that the interface is the core region for energy accumulation under thermal loading. The temporal evolution curve in Figure 6-3 shows that the dissipation energies in intragranular (Wc_I) and intergranular (Wc_II) regions increase synergistically, with the total effective dissipation energy eventually exceeding 1000 J/m³. This reflects the composite energy dissipation mechanism of "intragranular slip and intergranular sliding". Such energy concentration and accumulation directly correspond to the low-lifetime regions at the interface observed in the previous failure cycle diagram, establishing a logical chain of "energy dissipation → damage accumulation → life degradation". For life testing, the damage degree can be quickly estimated by monitoring the growth rate of interface dissipation energy (e.g., the increase within 60 min), and thermal cycle parameters (such as temperature change rate and holding time) can be optimized to delay energy accumulation.

3.4. Metallographic Analysis of Solder Joints

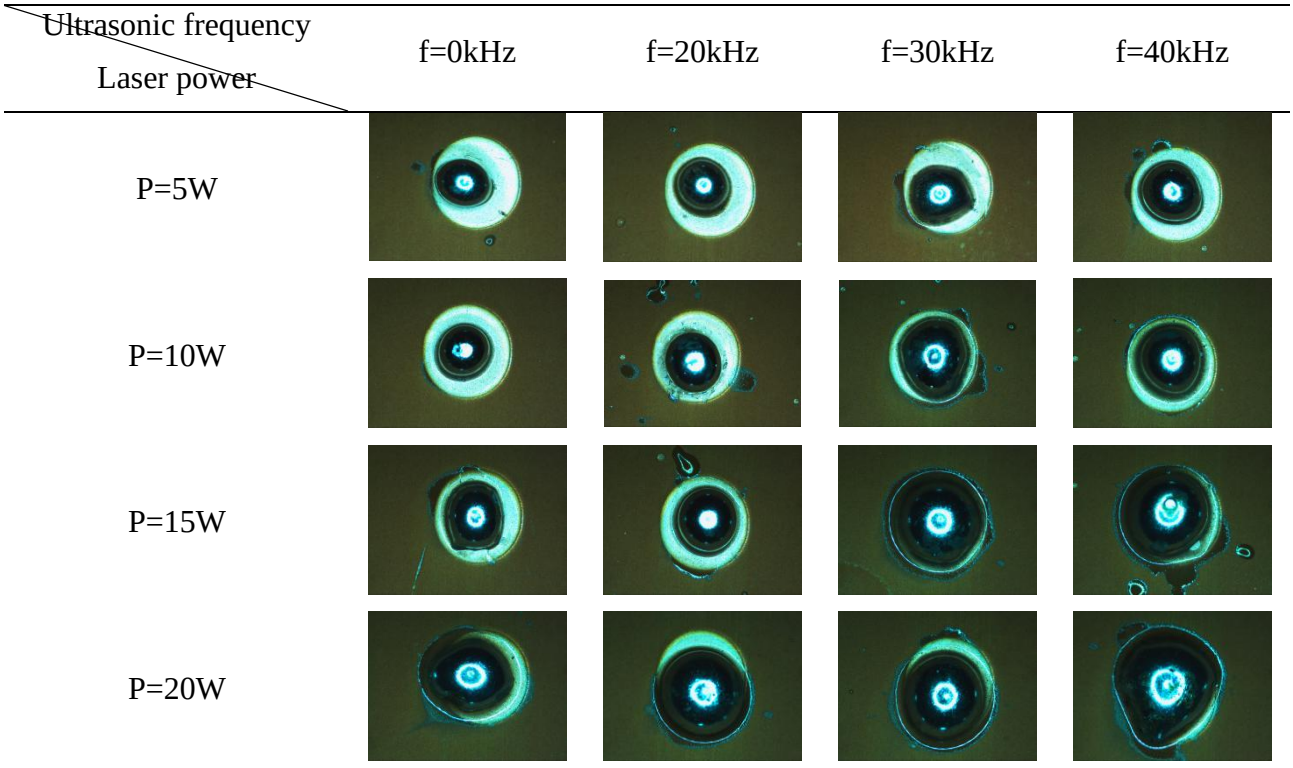

Figure 7. Metallographic images of solder joints under different ultrasonic frequencies and laser powers

Figure 7 shows the metallographic images of solder joints under different ultrasonic frequencies and laser powers. Without ultrasonic loading, laser power promotes solder melting by increasing heat flux, gradually improving the wettability and spreadability of solder joints without causing solder splashing, reflecting the positive effect of pure thermal driving. At low laser power (5W), due to insufficient power density, the solder melting degree is limited; even with ultrasonic vibration, the acoustic streaming effect cannot overcome the "low melting state constraint", resulting in insignificant improvement in wettability. As the laser power increases (15W, 20W), enhanced heat input brings the solder into a fully molten state, allowing the stirring effect of ultrasonic acoustic streaming to function effectively, thus synchronously improving wettability and spreadability: the combinations of 15W laser power with 30–40kHz ultrasonic frequency, and 20W laser power with 20–40kHz ultrasonic frequency exhibit good wettability. However, when the laser power is 15W and the ultrasonic frequency is 40kHz, the strong acoustic streaming caused by excessively high ultrasonic frequency disrupts the flow balance of molten solder, leading to solder splashing; for 20W laser power, under low ultrasonic frequencies (0–30kHz), the coupling imbalance between high-power-driven molten fluidity and ultrasonic flow field results in solder aggregation and partial exposure of the substrate, while at 40kHz, ultrasound reactivates the uniformity of the molten solder flow field, restoring complete spreading. These observations reveal the synergistic matching mechanism of the laser-ultrasonic composite energy field: low power requires overcoming the critical melting state, while high power needs to regulate acoustic streaming to maintain flow balance, providing an energy-kinetics coupling theoretical basis for optimizing welding parameters.

4. CONCLUSIONS

This study investigates the microstructure formation mechanism of Cu-Sn alloys and the action law of composite energy fields during ultrasonic-assisted laser soldering through experiments and numerical simulations, with the main conclusions as follows:

(1) Synergistic mechanism of laser and ultrasound: Laser power is the core driver of heat input. As laser power increases from 5W to 20W, the maximum temperature of the molten pool rises from 111.47°C to 291.79°C, directly determining the degree of solder melting. Ultrasonic frequency regulates molten pool dynamics through the acoustic streaming effect, with approximately 30kHz approaching the resonance frequency of the molten pool, increasing the flow velocity to 0.51mm/s, significantly enhancing convective heat transfer, improving temperature uniformity, and suppressing local overheating.

(2) Solder joint formation and defect control: At low power (5W), ultrasound has limited effect on improving wettability due to insufficient solder melting. At medium to high powers (10–20W), ultrasound reduces the surface tension of the solder and promotes spreading. Specifically, the combinations of 15W laser power with 30–40kHz ultrasonic frequency and 20W laser power with 20–40kHz ultrasonic frequency show good wettability. However, when the laser power is 15W and the ultrasonic frequency is 40kHz, strong acoustic streaming disrupts flow balance, causing solder splashing; for 20W laser power, ultrasonic frequencies of 0–30kHz easily lead to solder aggregation due to flow field coupling imbalance, while 40kHz ultrasound mitigates this issue.

(3) Interface reliability and lifetime characteristics: The interfacial IMC layer exhibits significant creep strain (on the order of 10^{-3}–10^{-4}) due to thermal expansion mismatch, making it the weak zone for fatigue failure. Ultrasonic assistance reduces the peak creep strain at the interface by 1–2 orders of magnitude through refining the IMC layer and reducing stress concentration, while also improving joint mechanical properties by inhibiting grain boundary coarsening. Accelerated life tests demonstrate that both the energy method and strain-life method identify the interface edge as the initiation site of failure, and ultrasonic assistance increases the number of interface failure cycles by 10%–30%. The core mechanism is that ultrasonic acoustic streaming promotes uniform heat diffusion,

reducing the accumulation rate of interface dissipation energy (the increase in dissipation energy within 60 min is 25% lower than that without ultrasound).

(4) Optimized process parameters: Considering solder joint formation quality and reliability, the optimal process combination is 10–15W laser power with 30kHz ultrasonic frequency. This combination achieves a molten pool flow velocity of 0.5–0.7mm/s, uniform temperature distribution (130–400°C), controls the IMC layer thickness within 1–5μm, and avoids significant splashing or aggregation defects, meeting the service requirements of fatigue resistance and high toughness for solder joints in electronic packaging.

This study clarifies the regulatory effects of the laser-ultrasonic composite energy field on the microstructure formation and reliability of Cu-Sn alloys, providing theoretical support and experimental basis for parameter optimization of high-precision, high-reliability soldering processes in electronic manufacturing.

ACKNOWLEDGMENT

This work is financially supported by the Wenzhou basic scientific research project (Grant NO. G2023031).

REFERENCES

[1] Lee J Y, Ju J E, Lee C, et al. Novel fabrication techniques for ultra-thin silicon based flexible electronics [J]. International Journal of Extreme Manufacturing, 2024, 6(4): 042005.

[2] Lau J H. State of the art of lead-free solder joint reliability [J]. Journal of Electronic Packaging, 2021, 143(2): 020803.

[3] Cao B, Su T, Yu S, et al. Active learning accelerates the discovery of high strength and high ductility lead-free solder alloys [J]. Materials & Design, 2024, 241: 112921.

[4] Lin J, Lu J, Xu J, et al. Welding quality analysis and prediction based on deep learning [C]//2021 4th World Conference on Mechanical Engineering and Intelligent Manufacturing (WCMEIM). IEEE, 2021: 173-177.

[5] Zhang C, Fan Z, Dai Y, et al. Path Planning of Laser Soldering System Based on Intelligent Algorithm [J]. Sensors, 2022, 22(21): 8120.

[6] Nishikawa H, Iwata N. Formation and growth of intermetallic compound layers at the interface during laser soldering using Sn–Ag Cu solder on a Cu Pad [J]. Journal of Materials Processing Technology, 2015, 215: 6-11.

[7] Kunwar A, An L, Liu J, Shang S, et al. A data-driven framework to predict the morphology of interfacial Cu6Sn5 IMC in SAC/Cu system during laser soldering. J Mater Sci Technol 2020; 50:115.

[8] Bachok Z, Abas MA, Nazarudin MZH, Zahiri SA, et al. Effect of different solder volumes on the laser soldering process: numerical and experimental investigation. J Electron Packag 2022;144.

[9] Kago K, Suetsugu K, Hibino S, et al. Novel ultrasonic soldering technique for lead-free solders [J]. Materials transactions, 2004, 45(3): 703-709.

[10] Leng X, Yang W, Zhang J, et al. High-performance joining technology for aluminium matrix composites using ultrasonic-assisted brazing [J]. Materials Science and Technology, 2018, 34(6): 660-663.